



Lithiophilic Protective Dual Layer Enabling Stable Electrodeposition of Lithium at High Current Density

Hee-Joo Choi,¹ Ji-Wan Kim,² Hongyeul Bae,³ Jinhong Kim,³ and Dong-Won Kim^{1,2,z} 

¹Department of Battery Engineering, Hanyang University, Seoul 04763, Republic of Korea

²Department of Chemical Engineering, Hanyang University, Seoul 04763, Republic of Korea

³LiB Materials Research Center, POSCO HOLDINGS, Gyeongsangbuk-do 37673, Republic of Korea

Lithium (Li) is an ideal anode material for rechargeable batteries and thus manufacturing Li metal is crucial for the practical development of Li metal batteries. Electrodeposition is an efficient technique for producing ultrathin and scalable Li metal electrodes. However, the dendritic growth and the side reactions of Li with electrolyte during the electrodeposition are the main obstacles to overcome. In this study, we designed a pre-coated protective dual layer (PDL) composed of a poly(ethylene oxide)-based solid polymer electrolyte (SPE) and a polydopamine-coated cellulose membrane (PD-CM). The adhesive and ion-conductive SPE layer suppressed the growth of Li dendrites and side reactions with liquid electrolyte. The PD-CM layer with high porosity and lithiophilicity promoted a facile and uniform Li-ion flux. By applying the pre-coated PDL, Li was uniformly electrodeposited on the Ag-coated Cu at a high current density of 6 mA cm⁻². The Li/LiFePO₄ cell composed of an electrodeposited Li anode with PDL and a LiFePO₄ cathode was assembled without an additional separator, and its cycling performance was evaluated. The cell initially delivered a high discharge capacity of 154.8 mAh g⁻¹ at 45 °C and exhibited excellent cycling stability with a capacity retention of 97.0% after 200 cycles.

© 2024 The Electrochemical Society ("ECS"). Published on behalf of ECS by IOP Publishing Limited. All rights, including for text and data mining, AI training, and similar technologies, are reserved. [DOI: [10.1149/1945-7111/ad8482](https://doi.org/10.1149/1945-7111/ad8482)]

Manuscript submitted August 6, 2024; revised manuscript received September 20, 2024. Published October 17, 2024.

Supplementary material for this article is available [online](#)

With the expansion of battery applications such as electric vehicles and energy storage systems, the demand for high energy density lithium (Li) batteries has increased. One of the most promising strategies for achieving high energy density is to use Li metal as an anode material owing to its high specific capacity and low electrode potential.^{1–3} To maximize the energy density of Li metal batteries, it is essential to use thin Li metal.^{4–7} However, producing ultrathin Li metal foil is challenging because of its intrinsic properties such as ductility and chemical instability.^{8,9} Various industrial processes such as extrusion, physical vapor deposition, Li powder casting, and electrodeposition have been employed to manufacture Li metal electrode.^{10–12} Electrodeposition is an efficient technique for fabricating ultrathin and scalable Li metal electrodes. In the electrodeposition process, the thickness of the Li metal can be easily controlled by adjusting the current density and electrodeposition time.¹³ In addition, the electrodeposition process can be conducted under mild temperature and atmospheric pressure conditions and offers the advantage of scalability because it can be easily applied to the roll-to-roll process. However, the fabrication of Li metal via electrodeposition presents several technical hurdles to its application in industrial processes. First, electrodeposition is usually conducted without external pressure, which results in nonuniform dendritic Li deposition.^{14–16} Moreover, electrodeposited Li is prone to side reactions with liquid electrolytes,¹⁷ and a high current density is required to reduce the electrodeposition time.¹⁸ Many studies have addressed these problems in the electrodeposition process, such as by designing new separator structures,¹⁹ optimizing electrolyte formulation,^{20,21} reforming appropriate substrate,^{22–25} and introducing protective layers.²⁶ The protective layer formed on the current collector can suppress the dendritic growth of Li and the side reactions of Li with the liquid electrolyte.^{27,28} However, most reported studies used a pressurized coin cell for electrodeposition, which cannot be applied to actual industrial processes.

In this study, we propose a pre-coated protective dual layer (PDL) for the uniform electrodeposition of Li metal onto an Ag-coated Cu substrate under high current density and atmospheric pressure. The dual layer was prepared by pressing the bottom and top layers. The bottom layer was a semi-interpenetrating polymer

network (semi-IPN)-type solid polymer electrolyte (SPE) based on poly(ethylene oxide) (PEO), cross-linked poly(ethylene glycol) diacrylate (PEGDA), and lithium bis(trifluoromethanesulfonyl) imide (LiTFSI). According to previous report, the semi-IPN polymer electrolyte composed of PEO, PEGDA and LiTFSI exhibited high ionic conductivity, good stability toward Li metal, and high electrochemical stability.²⁹ The bottom layer physically suppressed dendritic Li growth and the deleterious reactions of Li with the liquid electrolyte during electrodeposition, and its highly adhesive properties helped integrate the current collector and the top layer.³⁰ The top layer, a lithiophilic polydopamine-coated cellulose membrane (PD-CM), induced fast and uniform Li⁺-ion flux through the membrane and suppressed short-circuit between the two electrodes.^{31,32} Various electrochemical characteristics were investigated to understand the electrodeposition behavior of Li using the PDL. Furthermore, the electrodeposited Li anode with PDL and LiFePO₄ (LFP) cathode was applied to the lithium metal battery without an additional separator, and its cycling performance was evaluated. The cell delivered a high initial discharge capacity of 154.8 mAh g⁻¹ with a capacity retention of 97.0% after 200 cycles at 0.5 C and 45 °C.

Experimental Method

Materials.—PEO (MW = 600,000), PEGDA (MW = 575), dopamine hydroxyl, and anhydrous dimethylformamide (DMF) were purchased from Sigma-Aldrich. PEO and LiTFSI (Dongwha Electrolyte) were dried at 90 °C for 6 h before use. Azobisisobutyronitrile (AIBN) was purchased from Junsei Co. and used as a thermal initiator. A polyethylene (PE) separator (Asahi ND 420) and cellulose membrane (thickness: 35 μm, NKK) were vacuum dried for 12 h at 80 °C before use. The liquid electrolyte (battery grade, Enchem) was composed of dimethoxyethane, LiFSI, lithium nitrate, and fluoroethylene carbonate in a mass ratio of 71.2:27.6:0.6:0.6.

Preparation of protective dual-layer.—The Ag-coated copper was used as a current collector to facilitate Li electrodeposition.³³ The PDL was fabricated by integrating semi-IPN-type solid polymer electrolyte as the bottom layer and PD-CM as the top layer. The bottom layer was prepared using the solution-casting method. PEO and LiTFSI were dissolved and stirred in an anhydrous DMF at

^zE-mail: dongwonkim@hanyang.ac.kr

80 °C for 6 h. Once the solution became homogeneous, PEGDA (25 wt% of PEO) and a trace amount of AIBN were added into the precursor. The amount of LiTFSI was determined to maintain a [repeating EO units]: [LiTFSI] = 10:1. The precursor solution was casted on the Ag-coated Cu substrate and kept at 90 °C for 12 h in a vacuum oven to drive thermal cross-linking of PEGDA and remove the residual solvent. The obtained SPE was 8 μm thick and well adhered to the current collector. The top layer (PD-CM) was prepared by dip-coating the cellulose membrane in a tris-buffer solution (pH 8.5) containing dopamine hydroxyl (2 g l⁻¹) at 45 °C for 12 h. As polydopamine was formed, the cellulose membrane gradually turned dark gray. The PD-CM was then washed with ethanol and dried at 70 °C for 12 h. The prepared bottom and top layers were finally adhered together by roll pressing to obtain the PDL. After roll pressing, the thickness of PDL was about 42 μm.

Cell assembly.—Li electrodeposition was performed using a homemade electrodeposition cell (ED cell). The ED cell was composed of Li foil as the Li source, a liquid electrolyte, and an Ag-coated Cu current collector in a Teflon cylinder (Fig. S1). The electrodeposition was performed on the Ag-coated Cu without and with PDL at constant current density of 6 mA cm⁻² and 45 °C. The amount of total charge during electrodeposition was set to be 4 mAh cm⁻², corresponding to the thickness of 20 μm. Electrodeposited Li metal with PDL was used to assemble an Li/LFP cell without an additional separator. The cell was assembled by stacking the electrodeposited Li metal with the PDL and LFP cathode (92.0 wt % LFP, active mass: 13 mg cm⁻²) on Al foil in the coin cell and injecting 10 μl of liquid electrolyte into the cell. For comparison, an Li/PE separator/LFP cell was also assembled by sandwiching the PE separator between the electrodeposited Li metal without the PDL and the LFP cathode, and injecting the same amount of liquid electrolyte.

Characterization and measurements.—The conversion of PEGDA after thermal cross-linking was calculated by ¹H nuclear magnetic resonance (NMR) spectroscopy using an NMR spectrometer (VNMRs 600 MHz, Varian). Fourier-transform infrared (FT-IR) spectroscopy was conducted using a Nicolet iS50 spectrometer (Thermo Fisher Scientific Inc.) in the wavenumber range of 400–4000 cm⁻¹ to confirm the coating of polydopamine on cellulose membrane. Field-emission scanning electron microscopy (FE-SEM; Verios G4UC, FEI) was used to examine the morphologies of the protective layer and deposited Li metal. Electrochemical impedance spectroscopy (EIS) was performed in the frequency range of 0.01 Hz to 1 MHz at an amplitude of 10 mV using an AC impedance

analyzer (ZIVE MP1, WonATech Co., Ltd). A cell assembled with Ag-coated Cu as the working electrode and Li metal as the counter and reference electrodes was used for linear sweep voltammetry (LSV) and cyclic voltammetry (CV) at a scan rate of 1 mV s⁻¹. The Li/LFP cell was cycled in the voltage range of 3.0–3.8 V at 45 °C with a battery cycler (WBCS 3000, WonATech Co., Ltd).

Results and Discussion

Figure 1 shows a schematic of the preparation of a PDL composed of bottom and top layers. The bottom layer was a thin solid polymer electrolyte film based on a semi-IPN composed of PEO and cross-linked PEGDA. The semi-IPN structure provided high mechanical strength to suppress the dendritic growth of Li and prevented the elution of linear PEO into the liquid electrolyte.^{34,35} LiTFSI was added to the bottom layer to make it ion-conductive and sticky by reducing the crystallinity of the PEO. The PD-CM was chosen as the top layer to achieve a uniform Li⁺-ion flux to the bottom layer and to suppress the short-circuit between the two electrodes. The polydopamine coated on the cellulose membrane can interact with Li⁺ ions via its polar carbonyl groups, which promote homogeneous flux through the PD-CM layer.³¹ The two layers were integrated by roll pressing and could not be separated because of the highly adhesive property of the bottom layer.

The surface and cross-sectional SEM images of the bottom layer are presented in Figs. 2a and 2b, respectively. The bottom layer was densely coated with Ag-coated Cu without any void spaces or pits. The conversion of PEGDA in the bottom layer was determined using ¹H-NMR spectroscopy (Fig. 2c), as previously reported.^{36,37} P-xylene was added to the precursor as an internal standard, and its peak appeared at 7.05 ppm in the ¹H NMR spectrum. Several peaks observed in the range of 5.8–6.5 ppm (peak a, b, c) corresponded to vinyl group of PEGDA in the precursor solution. The PEGDA conversion after thermal curing was calculated using the following equation:

$$\text{Conversion (\%)} = \left(1 - \frac{1}{3} \left(\frac{I_f^a}{I_0^a} + \frac{I_f^b}{I_0^b} + \frac{I_f^c}{I_0^c} \right) \right) \times 100$$

where I_0^a , I_0^b , and I_0^c are the initial intensities of protons a, b, and c in the precursor, respectively, and the I_f^a , I_f^b , and I_f^c are the final intensities of protons a, b, and c in the semi-IPN obtained after thermal curing, respectively. As shown in figure 2c, the vinyl peaks of PEGDA almost disappeared after the cross-linking reaction. By

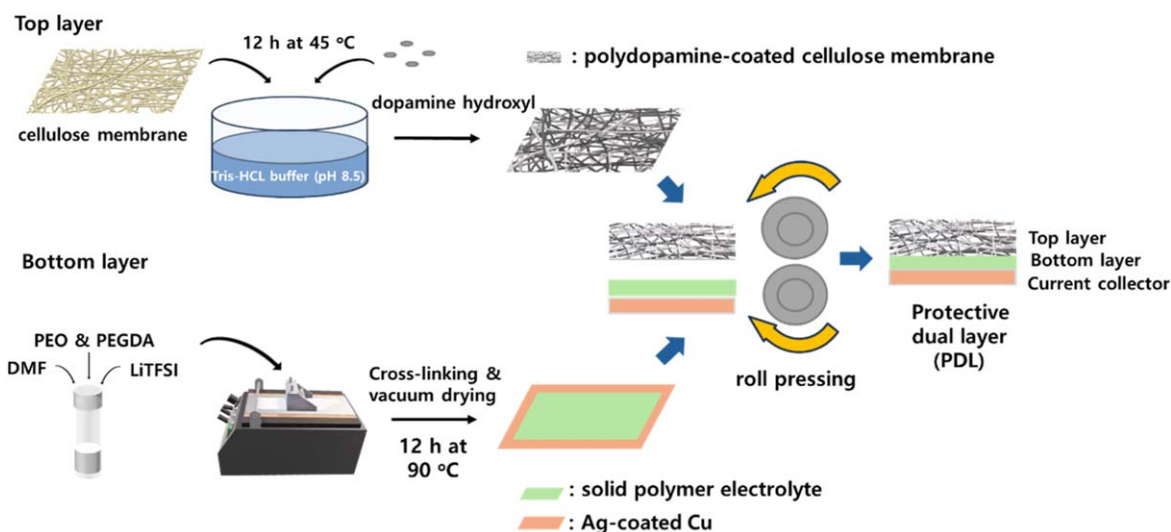


Figure 1. Schematic presentation for preparing the protective dual layer composed of bottom layer and top layer.

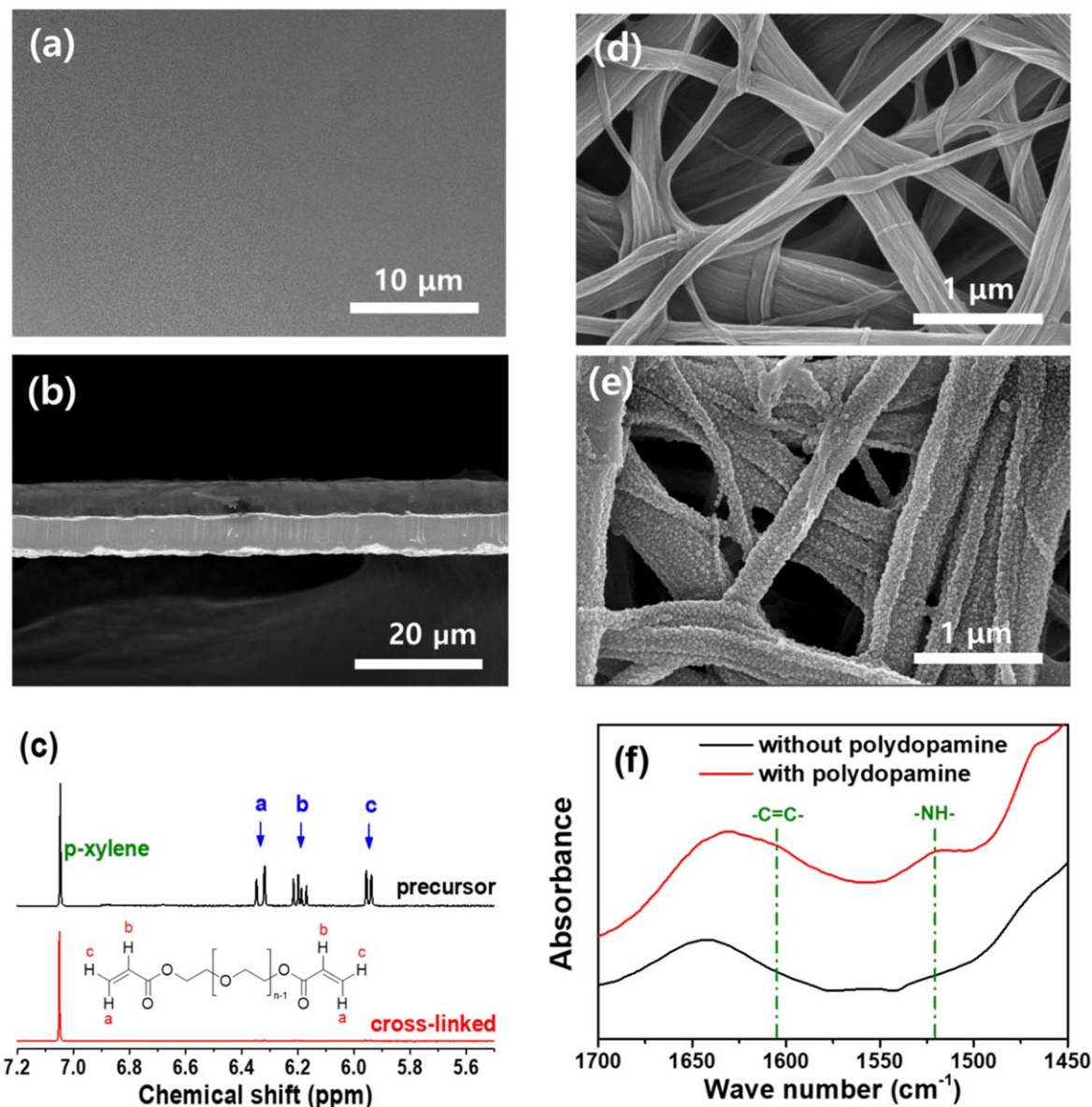


Figure 2. (a) Surface and (b) cross-sectional SEM images of the solid polymer electrolyte (bottom layer). (c) ¹H NMR spectra of precursor and solid polymer electrolyte obtained by thermal curing. Surface SEM images of (d) pristine cellulose membrane and (e) polydopamine-coated cellulose membrane (top layer). (f) FT-IR spectra of pristine and polydopamine-coated cellulose membranes.

substituting the obtained intensities into the above equation, the conversion of PEGDA was determined to be 99.7%, indicating that all the PEGDA was consumed by the free-radical reaction. Figures 2d and 2e show the SEM images of the cellulose membrane before and after polydopamine coating, respectively. Because polydopamine is strongly bonded to the cellulose membrane through hydrogen bonding, as depicted in Fig. S2, all fibers in the cellulose membrane were well-coated with grain-shaped polydopamine. FT-IR spectra were obtained to confirm the polydopamine coating on the cellulose membrane (Fig. 2f). The new absorption peaks observed at 1517 and 1605 cm⁻¹ in the PD-CM correspond to the stretching vibration peaks of -NH- and -C=C-, respectively, indicating the successful coating of polydopamine on the cellulose membrane.³⁸

Figure 3a shows a cross-sectional SEM image of the PDL obtained after roll pressing. From the image, the thicknesses of bottom and top layer were determined to be 7 μm and 35 μm, respectively. That is, the total thickness of PDL was 42 μm. When the thickness of PDL was less than 42 μm, the mechanical property of PDL was too weak, resulting in short-circuit during cycling of the

Li/LiFePO₄ cell without an additional separator. Figure 3b shows the ionic conductivities of the PE separator and PDL soaked in the same amount of liquid electrolyte as a function of temperature. The PDL exhibited higher ionic conductivities than the PE separator, which can be attributed to the higher porosity and electrolyte affinity of the PD-CM compared with the PE separator.³⁹ The porosity of lithiophilic PD-CM was much higher (69%) than that of hydrophobic PE separator (40%), resulting in higher uptake of electrolyte solution in PDL (185%) compared to PE separator (63%). The high ionic conductivity of PDL is expected to promote fast Li-ion transport and induce the uniform electrodeposition of Li, even at high current densities. The electrolyte affinity of PDL was investigated using contact-angle measurements. As shown in Fig. S3, the PDL exhibited a lower contact angle than the PE separator, indicating better wettability of the PDL. These results can be attributed to the high porosity of the cellulose membrane and the presence of polar groups in polydopamine.⁴⁰ The reductive stabilities of the PE separator and PDL soaked in the liquid electrolyte were evaluated using linear sweep voltammetry (Fig. 3c). They

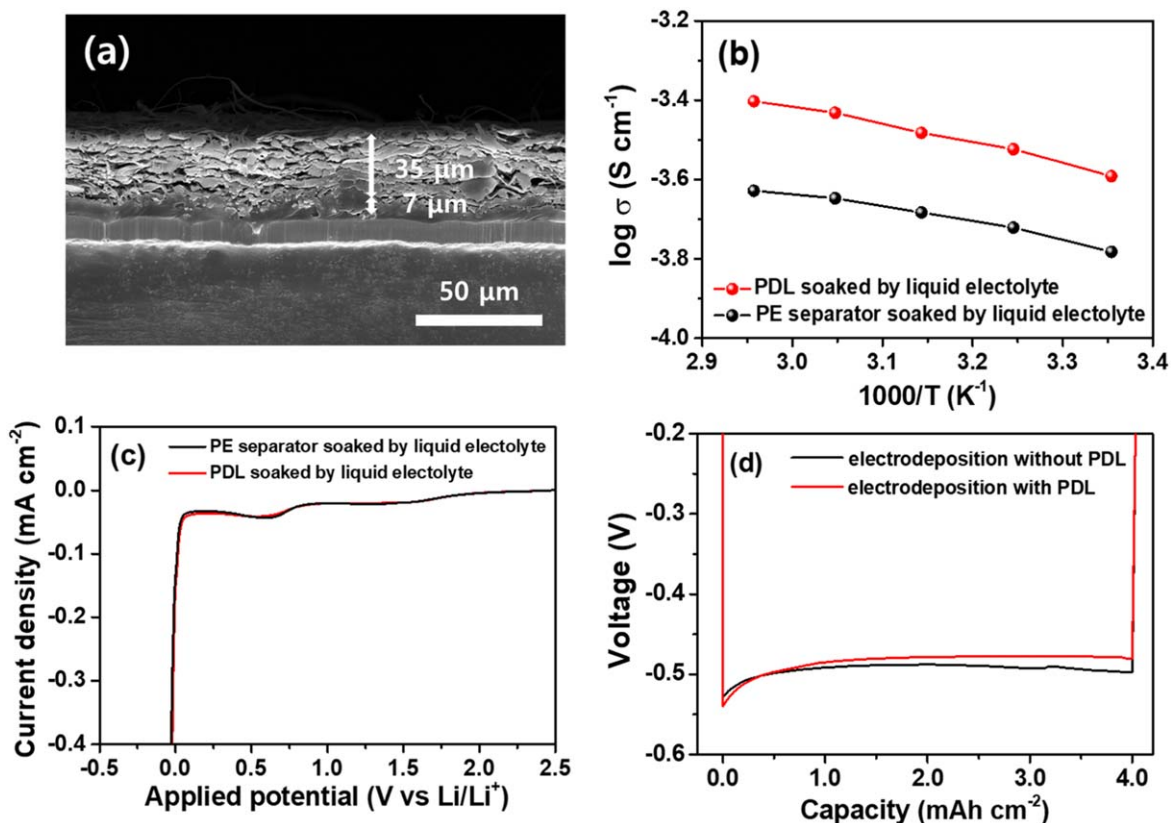


Figure 3. (a) Cross-sectional SEM image of the PDL and (b) ionic conductivities of PE separator and PDL soaked by liquid electrolyte. (c) Linear sweep voltammograms of the PE separator and PDL soaked by liquid electrolyte at a scan rate of 1.0 mV s^{-1} . (d) Voltage-capacity curves during electrodeposition onto Ag-coated Cu with and without PDL at 6 mA cm^{-2} .

exhibited the same cathodic peaks approximately 1.5 and 0.6 V, corresponding to the formation of solid electrolyte interphase (SEI) arising from the reductive decomposition of liquid electrolyte.^{41,42} These results suggest that PDL has sufficient reductive stability for the electrodeposition of Li^+ . The electrodeposition of Li was conducted onto the Ag-coated Cu at a current density of 6 mA cm^{-2} with a total capacity of 4 mAh cm^{-2} . Figure 3d shows the voltage profiles obtained during the electrodeposition of Li onto Ag-coated Cu with and without the PDL. The cells exhibited a relatively high overpotential ($\sim 0.5 \text{ V}$) owing to the high current density (6 mA cm^{-2}) and high resistance arising from the large distance ($\sim 1 \text{ cm}$) between the Ag-coated Cu and Li metal in the ED cell. When electrodeposition was performed on Ag-coated Cu without a PDL, the cell exhibited a fluctuating voltage behavior during the latter stage of electrodeposition because the inhomogeneous Li deposition hindered the Li^+ -ion flux.^{43,44} In contrast, Ag-coated Cu with a PDL displayed stable electrodeposition with a lower overpotential at the end of electrodeposition. When bare Cu was used as a substrate with a PDL for electrodeposition of Li instead of Ag-coated Cu, the overpotential was high compared to the Ag-coated Cu (Fig. S4a). Moreover, the electrodeposited Li on bare Cu exhibited moss-like and nonuniform morphology, as presented in Fig. S4b. These results suggest that the use of Ag-coated Cu allowed the uniform electrodeposition of Li by forming an alloy structure of Li and Ag, as previously reported.^{45,46}

Photographs and SEM images of electrodeposited Li are shown in Fig. 4. When employing Ag-coated Cu without a PDL, the Li metal electrodeposited on the current collector (Bare-Li) exhibited a bumpy and rough surface (Fig. 4a). As shown in the surface SEM image in Fig. 4b, the surface of Bare-Li was mossy and porous, indicating uneven Li deposition at a high current density. The average thickness of Bare-Li was approximately $300 \mu\text{m}$ (Fig. 4c),

which was much larger than $20 \mu\text{m}$ corresponding to the electrodeposition of 4 mAh cm^{-2} . The highly porous Li metal increases the contact area between the liquid electrolyte and the Li metal, may result in the acceleration of parasitic reactions. Figures 4d and S5a show photo and surface SEM images of the electrodeposited Li metal when using Ag-coated Cu with PDL. As shown in Fig. S5a, no Li was exposed outside the PDL, indicating that Li was electrodeposited under the PDL. The total thickness of electrodeposited Li electrode including current collector and PDL was about $75 \mu\text{m}$ (Fig. S5b). To examine the surface morphology of the electrodeposited Li in the PDL, the obtained electrode was immersed in DMF to remove the PDL. As shown in Fig. 4e, after removing PDL, the electrodeposited Li exhibited a dense and non-dendritic surface morphology. The cross-sectional SEM image revealed that the electrodeposited Li was $21 \mu\text{m}$ thick (Fig. 4f). The cross-sectional image of the electrodeposited Li with the PDL was further investigated by EDS elemental mapping (Fig. S6). In these figures, the deposited Li layer is indicated by a white dotted box. It is noticeable that the Ag element was also detected in the electrodeposited Li metal, indicating the formation of solid solution of Li and Ag during electrodeposition process. The mapping image of elemental C clearly confirmed that Li was electrodeposited under the PDL.

We investigated the deposition and stripping behavior of Li on Ag-coated Cu in a pressured coin cell instead of an ED cell under non-pressured conditions. In the absence of a PDL, a PE separator was inserted between the Li metal and the Ag-coated Cu to prevent short circuiting. Figures 5a and 5b depict the cyclic voltammograms of the Li/electrolyte/Ag-coated Cu cells assembled with PE and PDL at a scan rate of 1 mV s^{-1} , respectively. In the magnified cyclic voltammogram (Fig. S7), the cells exhibited the peaks of alloying and de-alloying of Li-Ag.^{47,48} The formation of SEI by reduction of liquid electrolyte was also observed.⁴⁹ When comparing the

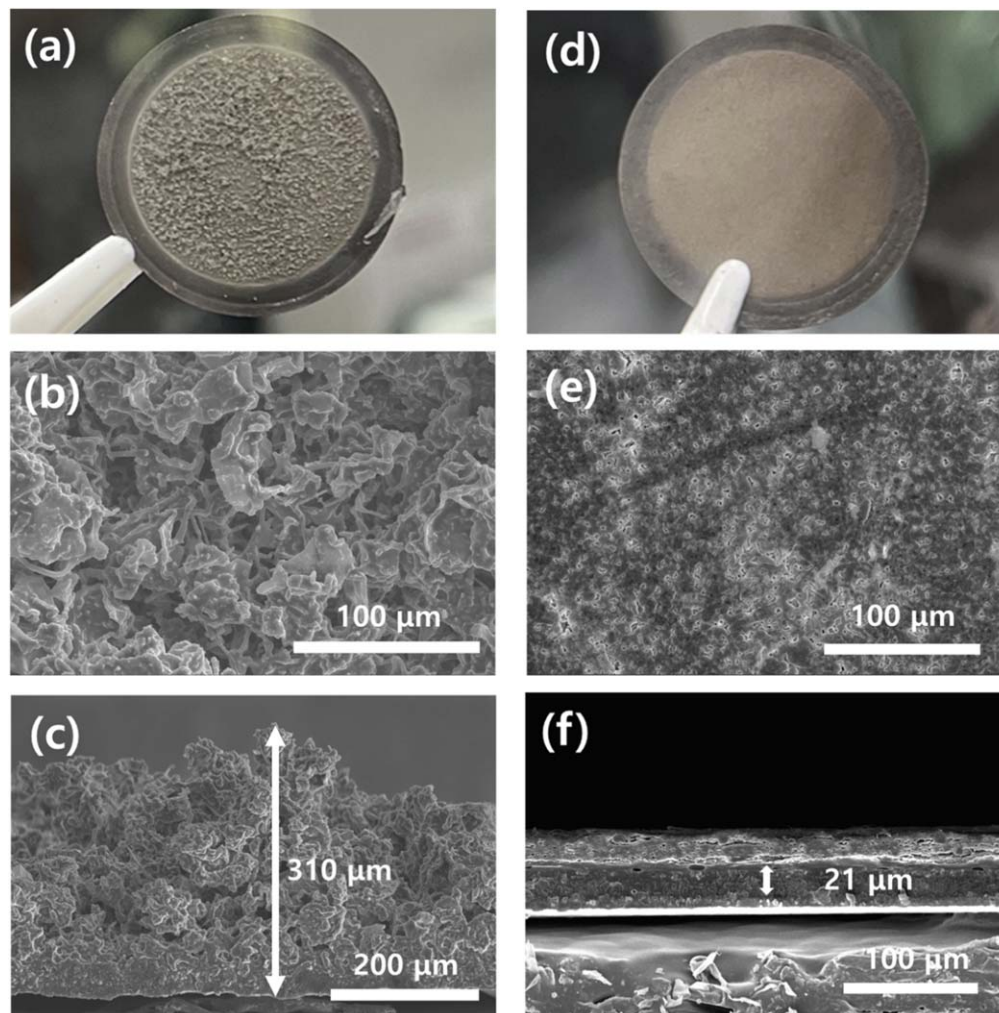


Figure 4. Photograph, surface and cross-sectional SEM images of Li metal electrodes obtained by electrodeposition onto the Ag-coated Cu without PDL (a–c) and with PDL (d–f).

electrodeposited capacity and the Coulombic efficiency (CE) of the two cells in the first cycle, the cell employing the PDL demonstrated a higher deposited capacity and CE than the cell with the PE separator, as shown in Fig. 5c. These results suggest that the deposition and stripping of Li are more favorable and stable on Ag-coated Cu with PDL than on the PE separator in the pressured coin cell. The exchange current density for charge transfer reaction ($\text{Li}^+ + e \leftrightarrow \text{Li}$) was determined from the Tafel plot. The Tafel plot describes how the current through an electrode depends on the potential difference between the electrode and the electrolyte for an electrochemical reaction. According to previous works,^{50,51} the higher exchange current density was observed for deposition and stripping of Li with lower charge transfer resistance, because it was under kinetic control. As shown in Fig. 5d, the electrodeposited Li with PDL exhibited a higher exchange current density than Bare-Li, indicating a facile charge transfer reaction. Figures 5e and 5f present the electrochemical impedance spectra of the symmetric Li/Li cells employing electrodeposited Li without and with the PDL, respectively, as a function of the storage time. The spectra are in the form of distorted semicircle composed of two semicircles. According to the previous studies, the semicircle at high frequency region is related with the resistance for Li^+ ion migration in the surface film formed on the Li electrode (R_f), and the semicircle in the mid-to-low frequency range can be attributed to the charge transfer resistance (R_{ct}).^{52,53} Thus, the interfacial resistance in the Li/Li cell is the sum R_f of and R_{ct} . As shown in figures, the electrodeposited Li without a

PDL (Bare-Li) showed a large increase in the interfacial resistance, while the electrodeposited Li with PDL exhibited a stable interfacial resistance after an initial slight increase. Because the Li metal is highly susceptible to side reactions including corrosion with liquid electrolyte (salts and solvents),⁵⁴ the increase in the interfacial resistance can be ascribed to the continuous occurrence of side reactions at the Li metal-liquid electrolyte interface. Accordingly, these results suggest that the presence of a PEO-based solid polymer electrolyte (bottom layer) formed on the Ag-coated Cu effectively suppresses the side reactions of Li with the liquid electrolyte. From these results, it was confirmed that the electrodeposited Li with PDL had fast charge transfer reaction kinetics and enhanced interfacial stability compared with Bare-Li. The repeated galvanostatic stripping/deposition of Li in the symmetric Li/Li cells was performed at a constant current density of 0.4 mA cm^{-2} with a cut-off capacity of 0.8 mAh cm^{-2} at 45°C to explore the applicability of PDL as a separator in the Li metal battery. As depicted in Fig. S8a, the voltage profiles of the cell employing electrodeposited Li with the PDL were quite stable, and its overpotential was much lower than that of the Bare-Li/PE separator/Bare-Li cell. The cell employing the PDL cycled stably over 2000 h without a noticeable increase in the overpotential and short-circuit, which demonstrates that the PDL can be used as a separator. When the current density was increased to 1.0 mA cm^{-2} with a cut-off capacity of 2.0 mAh cm^{-2} at 45°C (Fig. S8b), the electrodeposited Li without PDL showed a rapid increase in overpotential and eventually short-circuit after 100 h due

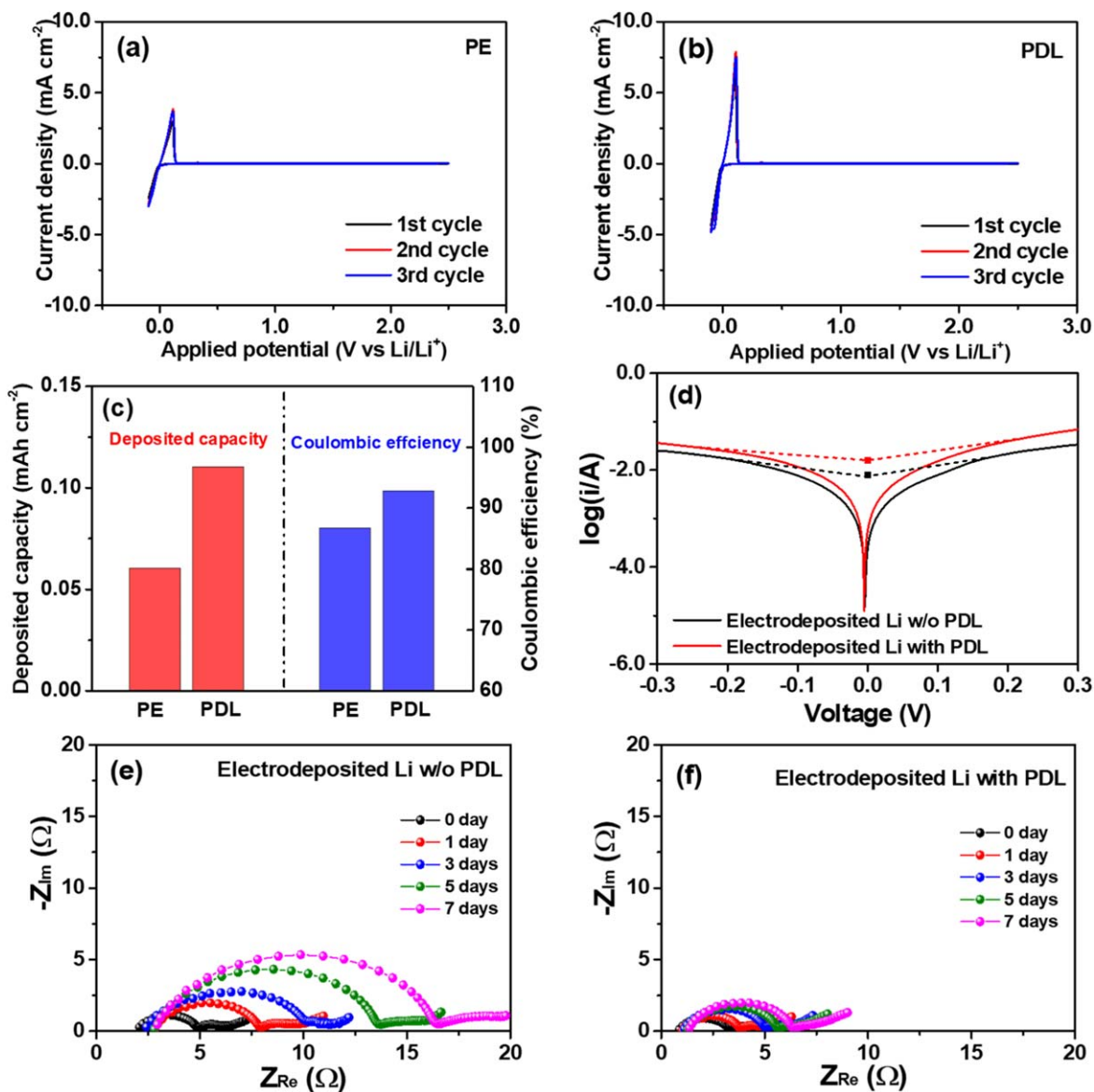


Figure 5. Cyclic voltammograms of the Li/electrolyte/Ag-coated Cu cells with (a) PE and (b) PDL at a scan rate of 1 mV s^{-1} , and (c) corresponding capacity and coulombic efficiency. (d) Tafel plots of the symmetric electrodeposited Li/electrolyte/ electrodeposited Li cells. Nyquist plots of the symmetric electrodeposited Li/electrolyte/ electrodeposited Li cells (e) without and (f) with PDL as a function of time.

to the dendritic growth of Li. In contrast, the electrodeposited Li with PDL exhibited stable cycling behavior without a noticeable increase in overpotential over 350 h.

We assembled an Li/LFP cell composed of an electrodeposited Li anode with PDL and an LFP cathode without an additional separator (Fig. S9a). Figure S10 presents the SEM image of LFP cathode, and corresponding EDS mapping images of P, C, and F elements. It reveals that cathode active material (P), conducting carbon (C), and poly(vinylidene fluoride) binder (F) are uniformly distributed within the cathode. As shown in cycling results (Fig. 6a), the cell employing PDL delivered a high initial discharge capacity of 154.8 mAh g^{-1} at 45°C and exhibited excellent capacity retention at 0.2 C charge and 0.5 C discharge cycling. In contrast, the Bare-Li/LFP cell employing a PE separator (Fig. S9b) showed large capacity fading and unstable cycling behavior, as can be seen in Fig. 6b. This result can be attributed to the side reactions of highly porous Bare Li with a high surface area (Fig. 4c) and gradual loss of Li due to its dendritic growth during cycling. We compared the cycling performance of the electrodeposited Li/LFP cell with that of Li metal

($20 \mu\text{m}$, Honjo Metal)/LFP cell. As presented in Fig. S11, although the initial capacities of the two cells were almost the same, the cell employing electrodeposited Li and PDL showed better characteristics in terms of cycling stability. Figure 6c presents the discharge curves of the electrodeposited Li with PDL/LFP cell at different C rates and 45°C , and the rate capability of two cells are compared in Fig. 6d. As expected, the cell employing electrodeposited Li with PDL displayed better high-rate performance than the cell using Bare-Li and PE separator, which can be ascribed to the lower cell resistance, including bulk resistance and interfacial resistance, as previously discussed.

Based on our results, the electrodeposition of Li on Ag-coated Cu and its cycling behavior are schematically presented in Fig. 7. By pre-coating the PDL onto the current collector, we could fabricate the uniformly electrodeposited Li metal under atmospheric pressure condition at a high current density of 6 mA cm^{-2} . The Li/LFP cell employing the electrodeposited Li metal with the PDL exhibited excellent cycling stability and better high-rate performance than the cell assembled with Bare-Li and PE separator.

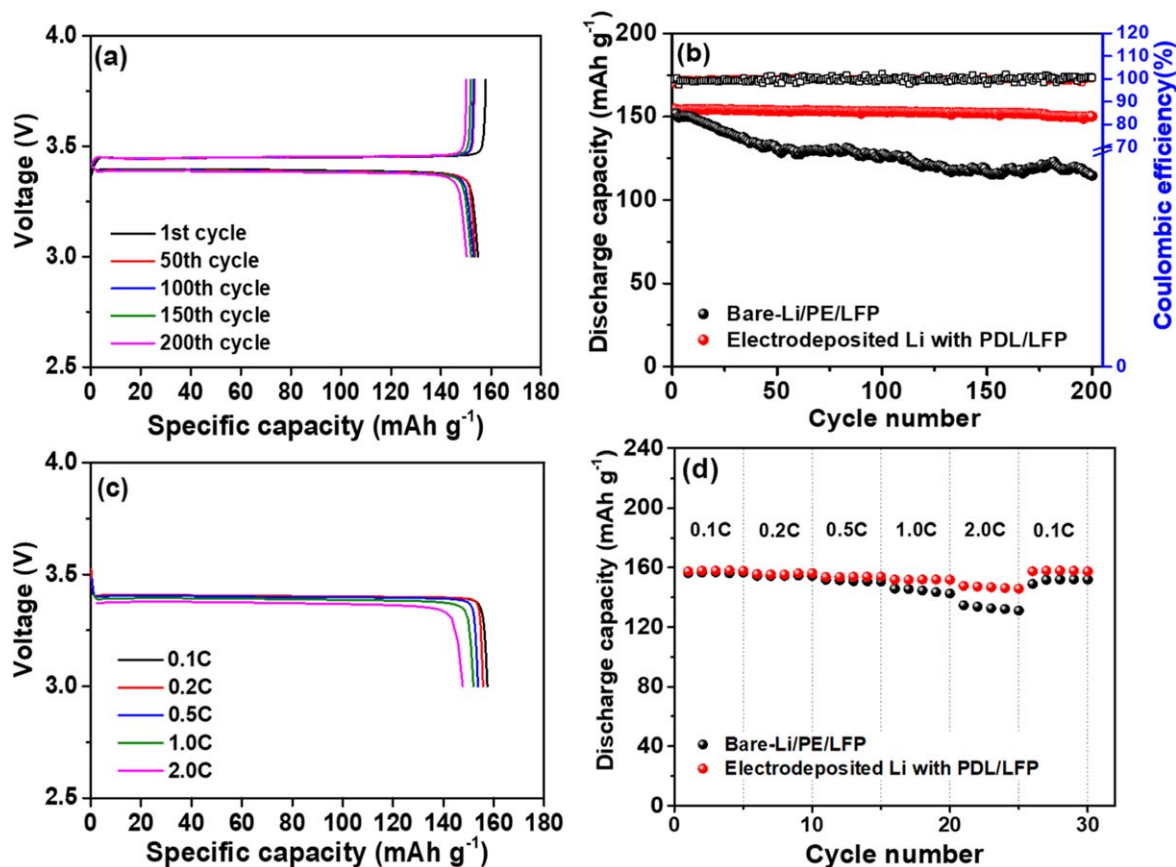


Figure 6. (a) Voltage profiles of the electrodeposited Li with PDL/LFP cell and (b) cycling performance of the Li/LFP cells with different Li anode and separator at 0.2 C charge and 0.5 C discharge cycle. (c) Discharge curves of the electrodeposited Li with PDL/LFP cell at 45 °C and (d) discharge capacities of the Li/LFP cells as a function of C rate. (1 C = 2.0 mAh cm⁻²).

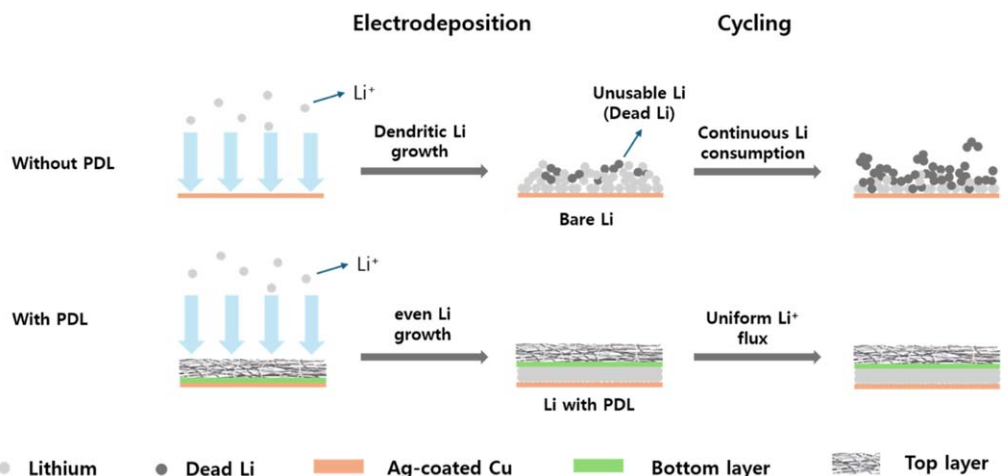


Figure 7. Schematic presentation for the electrodeposition of Li on the Ag-coated Cu and the cycling behavior of the electrodeposited Li without and with PDL.

Conclusions

In this study, we fabricated an ionically conductive and lithophilic PDL on the Ag-coated Cu current collector for the electrodeposition of Li. The PDL consisted of a PEO-based semi-IPN-type solid polymer electrolyte as the bottom layer and a lithophilic polydopamine-coated cellulose membrane as the top layer. The bottom layer minimized the parasitic reactions of the deposited Li with the liquid electrolyte and suppressed dendritic growth of Li during electrodeposition. The top layer improved the ionic conductivity and promoted uniform Li-ion flux at a high current density.

As a result, Li was uniformly electrodeposited on the Ag-coated Cu under PDL. The Li/LFP cell employing the electrodeposited Li metal with PDL exhibited a high initial discharge capacity of 154.8 mAh cm⁻² at 45 °C and an excellent cycling stability with a capacity retention of 97.0% after 200 cycles at 0.2 C charge/0.5 C discharge cycling.

Acknowledgments

This work was supported by POSCO Holdings.

ORCID

Dong-Won Kim  <https://orcid.org/0000-0002-1735-0272>

References

- X.-B. Cheng, R. Zhang, C.-Z. Zhao, and Q. Zhang, "Toward safe lithium metal anode in rechargeable batteries: a review." *Chem. Rev.*, **117**, 10403 (2017).
- P. Albertus, S. Babinec, S. Litzelman, and A. Newman, "Status and challenges in enabling the lithium metal electrode for high-energy and low-cost rechargeable batteries." *Nat. Energy*, **3**, 16 (2018).
- J. Liu et al., "Pathways for practical high-energy long-cycling lithium metal batteries." *Nat. Energy*, **4**, 180 (2019).
- W. Wu, W. Luo, and Y. Huang, "Less is more: a perspective on thinning lithium metal towards high-energy-density rechargeable lithium batteries." *Chem. Soc. Rev.*, **52**, 2553 (2023).
- B. Acebedo, M. C. Morant-Minana, E. Gonzalo, I. Ruiz de Larramendi, A. Villaverde, J. Rikarte, and L. Fallarino, "Current status and future perspective on lithium metal anode production methods." *Adv. Energy Mater.*, **13**, 2203744 (2023).
- R. Schmich, R. Wagner, G. Horpel, T. Placke, and M. Winter, "Performance and cost of materials for lithium-based rechargeable automotive batteries." *Nat. Energy*, **3**, 267 (2018).
- H. Zhang et al., "Preolithiation: a critical strategy towards practical application of high-energy-density batteries." *Adv. Energy Mater.*, **13**, 2300466 (2023).
- S.-K. Otto, T. Fuchs, Y. Moryson, C. Lerch, B. Mogwitz, J. Sann, J. Janek, and A. Henss, "Storage of lithium metal: the role of the native passivation layer for the anode interface resistance in solid state batteries." *ACS Appl. Energy Mater.*, **4**, 12798 (2021).
- H. Chen et al., "Free-standing ultrathin lithium metal-graphene oxide host foils with controllable thickness for lithium batteries." *Nat. Energy*, **6**, 790 (2021).
- C. Sun, X. Zhang, C. Li, K. Wang, X. Sun, and Y. Ma, "Recent advances in prelithiation materials and approaches for lithium-ion batteries and capacitors." *Energy Storage Mater.*, **32**, 497 (2020).
- F. Wang, J. Li, B. Wang, Y. Zhou, D. Wang, H. Liu, and S. Dou, "Preolithiation: a crucial strategy for boosting the practical application of next-generation lithium ion battery." *ACS Nano*, **15**, 2197 (2021).
- K. Schonherr, B. Schumm, F. Hippauf, R. Lissy, H. Althues, C. Leyens, and S. Kaskel, "Liquid lithium metal processing into ultrathin metal anodes for solid state batteries." *Chem. Eng. J. Adv.*, **9**, 100218 (2022).
- H. J. Kim, S. Choi, S. J. Lee, M. W. Seo, J. G. Lee, E. Deniz, Y. J. Lee, E. K. Kim, and J. W. Choi, "Controlled prelithiation of silicon monoxide for high performance lithium-ion rechargeable full cells." *Nano Lett.*, **16**, 282 (2016).
- X. Yin, W. Tang, I. D. Jung, K. C. Phua, S. Adams, S. W. Lee, and G. W. Zheng, "Insights into morphological evolution and cycling behavior of lithium metal anode under mechanical pressure." *Nano Energy*, **50**, 659 (2018).
- A. J. Louli, M. Genovese, R. Weber, S. G. Hames, E. R. Logan, and J. R. Dahn, "Exploring the impact of mechanical pressure on the performance of anode-free metal cells." *J. Electrochem. Soc.*, **166**, A1291 (2019).
- H. Kim, S.-H. Lee, J.-M. Kim, C. S. Yoon, and Y.-K. Sun, "High-energy-density, long-life li-metal batteries via application of external pressure." *ACS Energy Lett.*, **8**, 2970 (2023).
- K. Yoshii, H. Kiuchi, N. Taguchi, M. Shikano, E. Matsubara, and H. Sakaebe, "Effects of film formation on the electrodeposition of lithium." *ChemElectroChem*, **7**, 4336 (2020).
- L. T. Gao, P. Huang, and Z.-S. Guo, "Understanding charge-transfer and mass-transfer effects on dendrite growth and fast charging of Li metal battery." *J. Electrochem. Soc.*, **170**, 050512 (2023).
- J. Yang, C.-Y. Wang, C.-C. Wang, K.-H. Chen, C.-Y. Mou, and H.-L. Wu, "Advanced nanoporous separators for stable lithium metal electrodeposition at ultra-high current densities in liquid electrolytes." *J. Mater. Chem. A*, **8**, 5095 (2020).
- J. Seo, W. Jeong, M. Lim, B. Choi, S. Park, Y. Jo, J.-W. Lee, and H. Lee, "Electrodeposition-guided pre-passivation of Li-metal anode to enable long stable cycling of practical Li-metal batteries." *Energy Storage Mater.*, **60**, 102827 (2023).
- Y. Liang, W. Wu, D. Li, H. Wu, C. Gao, Z. Chen, L. Ci, and J. Zhang, "Highly stable lithium metal batteries by regulating the lithium nitrate chemistry with a modified eutectic electrolyte." *Adv. Energy Mater.*, **12**, 2202493 (2022).
- L. Fan, H. L. Zhuang, W. Zhang, Y. Fu, Z. Liao, and Y. Lu, "Stable lithium electrodeposition at ultra-high current densities enabled by 3D PMF/Li composite anode." *Adv. Energy Mater.*, **8**, 1703360 (2018).
- K. Y. Cho, S. H. Hong, J. Kwon, H. Y. Song, S. Kim, S. Jo, and K. Eom, "Effects of a nanometrically formed lithiophilic silver@copper current collector on the electrochemical nucleation and growth behaviors of lithium metal anodes." *Appl. Surf. Sci.*, **554**, 149578 (2021).
- S. Li et al., "Facile chemical fabrication of a three-dimensional copper current collector for stable lithium metal anodes." *J. Electrochem. Soc.*, **168**, 070502 (2021).
- S. Zhang, S. Xiao, D. Li, J. Liao, F. Ji, H. Liu, and L. Ci, "Commercial carbon cloth: an emerging substrate for practical lithium metal batteries." *Energy Storage Mater.*, **48**, 172 (2022).
- S. Lee, S. Cho, H. Choi, S. Kim, I. Jeoung, Y. Lee, T. Choi, H. Bae, J. H. Kim, and S. Park, "Bottom deposition enables stable all-solid-state batteries with ultrathin lithium metal anode." *Small*, **23**, 2311652 (2024).
- G. Wang, C. Chen, Y. Chen, X. Kang, C. Yang, F. Wang, Y. Liu, and X. Xiong, "Self-stabilized and strongly adhesive supramolecular polymer protective layer enables ultrahigh-rate and large-capacity lithium-metal anode." *Angew. Chem. Int. Ed.*, **59**, 2055 (2020).
- A. A. Assegie, J.-H. Cheng, L.-M. Kuo, W.-N. Su, and B.-J. Hwang, "Polyethylene oxide film coating enhances lithium cycling efficiency of an anode-free lithium-metal battery." *Nanoscale*, **10**, 6125 (2018).
- J. Jiang, H. Pan, W. Lin, W. Tu, and H. Zhang, "UV-induced semi interpenetrating polymer electrolyte membrane for elevated temperature all-solid-state lithium-ion batteries." *Mater. Chem. Phys.*, **236**, 121781 (2019).
- A. Maurel, M. Armand, S. Grugeon, B. Fleutot, C. Davoisne, H. Tortajada, M. Courty, S. Panier, and L. Dupont, "Poly(Ethylene Oxide)-LiTFSI solid polymer electrolyte filaments for fused deposition modeling three-dimensional printing." *J. Electrochem. Soc.*, **167**, 070536 (2020).
- Y. Fang, Z. Zhang, S. Liu, Y. Pei, and X. Luo, "Polydopamine-modified cellulose-based composite separator for inhibiting dendritic growth of lithium metal batteries." *Electrochim. Acta*, **475**, 143661 (2024).
- M.-L. Zhou, Z. Zhang, J. Xu, J. Wei, and Z.-Y. Yang, "PDA modified commercial paper separator engineering with excellent lithiophilicity and mechanical strength for lithium metal batteries." *J. Electroanal. Chem.*, **868**, 114195 (2020).
- Z. Zuo, L. Zhuang, J. Xu, Y. Shi, C. Su, P. Lian, and B. Tian, "Lithiophilic silver coating on lithium metal surface for inhibiting lithium dendrites." *Front. Chem.*, **8**, 109 (2020).
- J. Key, Y. Feng, J. Shen, P. Wang, H. Wang, H. Liang, R. Qiang, and S. Ji, "A highly crosslinked and conductive sulfur-rich copolymer with grafted polyaniline for stable cycling lithium-sulfur batteries." *J. Electrochem. Soc.*, **167**, 020530 (2020).
- A.-H. Ban, S.-J. Pyo, W. J. Bae, H.-S. Woo, J. Moon, and D.-W. Kim, "Dual-type gel polymer electrolyte for high-voltage lithium metal batteries with excellent cycle life." *Chem. Eng. J.*, **475**, 146266 (2023).
- S. Park, B. Jeong, D.-A. Lim, C. H. Lee, K. H. Ahn, J. H. Lee, and D.-W. Kim, "Quasi-solid-state electrolyte synthesized using a thiol-ene click chemistry for rechargeable lithium metal batteries with enhanced safety." *ACS Appl. Mater. Interfaces*, **12**, 19553 (2020).
- J.-W. Kim, M.-K. Oh, Y.-A. Kim, U. T. Nakate, E.-J. Kwon, S. Seo, W.-K. Kim, K.-H. Ryu, and D.-W. Kim, "Enhanced cycle life of lithium metal batteries via modulating the lithium-ion solvation sheath with a cross-linked gel polymer electrolyte." *J. Power Sources*, **598**, 234183 (2024).
- R. A. Zangmeister, T. A. Morris, and M. J. Tarlov, "Characterization of polydopamine thin films deposited at short times by autoxidation of dopamine." *Langmuir*, **29**, 8619 (2013).
- Q. Xu, Q. Kong, Z. Liu, J. Zhang, X. Wang, R. Liu, L. Yue, and G. Cui, "Polydopamine-coated cellulose microfibrillated membrane as high performance lithium-ion battery separator." *RSC Adv.*, **4**, 7845 (2014).
- M.-H. Ryou, Y. M. Lee, J.-K. Park, and J. W. Choi, "Mussel-inspired polydopamine-treated polyethylene separators for high-power li-ion." *Adv. Mater.*, **23**, 3066 (2011).
- W. Gu et al., "Lithium-iron fluoride battery with in situ surface protection." *Adv. Funct. Mater.*, **26**, 1507 (2016).
- J. Alvarado et al., "A carbonate-free, sulfone-based electrolyte for high-voltage Li-ion batteries." *Mater. Today*, **4**, 341 (2018).
- K.-H. Chen, K. N. Wood, E. Kazayak, W. S. Lepage, A. L. Davis, A. J. Sanchez, and N. P. Dasgupta, "Dead lithium: mass transport effects on voltage, capacity, and failure of lithium metal anodes." *J. Mater. Chem. A*, **5**, 11671.
- S. Xu, K.-H. Chen, N. P. Dasgupta, J. B. Siegel, and A. G. Stefanopoulos, "Evolution of dead lithium growth in lithium metal batteries: experimentally validated model of the apparent capacity loss." *J. Electrochem. Soc.*, **166**, A3456.
- K. Yan, Z. Lu, H.-W. Lee, F. Xiong, P.-C. Hsu, Y. Li, J. Zhao, S. Chu, and Y. Cui, "Selective deposition and stable encapsulation of lithium through heterogeneous seeded growth." *Nat. Energy*, **1**, 16010 (2016).
- C. Wei, H. Fei, Y. An, Y. Tao, J. Feng, and Y. Qian, "Uniform Li deposition by regulating the initial nucleation barrier via a simple liquid-metal coating for a dendrite-free Li-metal anode." *J. Mater. Chem. A*, **7**, 18861 (2019).
- S. Jin et al., "Solid-solution-based metal alloy phase for highly reversible lithium metal anode." *J. Am. Chem. Soc.*, **142**, 8818 (2020).
- J. Kim, I. Phiri, and S.-Y. Ryou, "Synergistically stabilizing thin li metal through the formation of a stable and highly conductive solid electrolyte interface and silver-lithium alloy." *ACS Appl. Mater. Interfaces*, **15**, 46765 (2023).
- D. Li, D. Danilov, Z. Zhang, H. Chen, Y. Yang, and P. H.-L. Notten, "Modeling the SEI-formation on graphite electrodes in LiFePO₄ batteries." *J. Electrochem. Soc.*, **162**, A858 (2015).
- G. Lu et al., "In-situ electrodeposition of nanostructured carbon strengthened interface for stabilizing lithium metal anode." *ACS Nano*, **16**, 9883 (2022).
- Y. Fan, J. Liao, D. Luo, Y. Huang, F. Sun, and J. Nan, "In situ formation of a lithiophilic surface on 3D current collectors to regulate lithium nucleation and growth for dendrite-free lithium metal anodes." *Chem. Eng. J.*, **453**, 139903 (2023).
- A. Funabiki, M. Inaba, and Z. Ogumi, "A.C. impedance analysis of electrochemical lithium intercalation into highly oriented pyrolytic graphite." *J. Power Sources*, **68**, 227 (1997).
- M. D. Levi, G. Salitra, B. Markovsky, H. Teller, D. Aurbach, U. Heider, and L. Heider, "Solid-state electrochemical kinetics of li-ion intercalation into Li_{1-x}CoO₂: simultaneous application of electroanalytical techniques SSCV, PITT, and EIS." *J. Electrochem. Soc.*, **146**, 1279 (1999).
- C. Jin et al., "A corrosion inhibiting layer to tackle the irreversible lithium loss in lithium metal batteries." *Nat. Commun.*, **14**, 8269 (2023).